UTEC MSE 69-161
December 1969

# DEVELOPMENT AND TESTING OF A BALLISTIC IMPACT LOADING DEVICE

by

Dolores Labranche Simonson



A thesis submitted to the faculty of the University of Utah in partial fulfillment of the requirements for the degree of

Master of Science

Division of Materials Science and Engineering
Department of Mechanical Engineering
University of Utah

June 1970

# DEVELOPMENT AND TESTING OF A BALLISTIC IMPACT LOADING DEVICE

by

Dolores Labranche Simonson

A thesis submitted to the faculty of the University of Utah in partial fulfillment of the requirements for the degree of

Master of Science

Division of Materials Science and Engineering
Department of Mechanical Engineering
University of Utah

June 1970

This Thesis for the

Master of Science Degree

by

Dolores Labranche Simonson

has been approved

November 1969

_____

Chairman, Supervisory Committee

_____

Supervisory Committee

_____

Supervisory Committee

_____

Chairman, Major Department

_____

Dean, Graduate School

## ACKNOWLEDGEMENTS

The results presented in this thesis were obtained in the course of the work conducted under a National Science Foundation Fellowship Grant GK-2188 with additional financial aid from NASA Grant NGR-45-003-029.

The author gratefully acknowledges the assistance from the principal investigator of the N.S.F. project, Dr. J. G. Byrne. The writer is indebted to Dr. G. A. Secor for his continual interest and his guidance in scratching the subject of waves in solids. Sincere appreciation is extended to Dr. K. L. DeVries for his teaching of a little EPR and a lot about materials. Without W. B. Jones' guidance, encouragement and support, this investigation would have been a complete disaster.

The author wishes to express thanks to Dieter Steinmann for his patience and his experience in building the test apparatus. Appreciation is extended to Mrs. Marvel Leader for the preparation of this manuscript.

The author thanks Terry Broadbent for her artistic contribution to the figures and for her never-ending bubbling personality.

Sincere appreciation is given to her parents, who were the backbone of her college education. Lastly, a thank you to Roger, her husband, for everything.

TABLE OF CONTENTS

LIST OF TABLES

LIST OF FIGURES

LIST OF FIGURES (continued)

LIST OF FIGURES (continued)

page

## ABSTRACT

A simple, economical device for producing cumulative shock loading in materials was investigated, designed, and tested. The device developed uses a ballistic impact-driven projectile to introduce high stress waves into the material. By adjusting design parameters, the impact time and load amplitude are varied to produce fracture with one load or several loads in PMMA rods. The wave front was examined as it travels through the PMMA rod and identified as approaching a square wave front. Materials other than PMMA were loaded to failure to demonstrate the scope of the loading apparatus. Fracture morphologies in the materials were microscopically examined and described with reference to established fracture modes.

# I. INTRODUCTION

Plane stress waves are used to study the response of materials at high stress levels.[1] High stress levels in this study are produced by a ballistic impact-driven projectile to approach shock conditions. Other techniques are available capable of producing high stress levels (shock), of which tapered brass horns,[2] lensed contact explosives,[3] and flyer plates driven by lensed explosives[4] are included. Each technique has its advantages and disadvantages. Without considering the cost or instrumentation, each has the disadvantage of long time delays between wave impulses. Ideally, experimental examination of shock waves introduced infinitely fast is desired.

With cumulative high stress loadings as the prime factor in this study, various methods were examined. With each method examined failing to produce confident fatigue results, a ballistic-driven projectile was developed to accommodate various cartridge loadings. When the bullet impacts the piston, a high energy stress wave propagates through the specimen to cause spalling at the end of the rod. In the scheme described, it is possible to vary both piston travel and bullet energy. The stress pulse generated in PMMA was a short duration, semi-rectangular pulse.

## II. FRACTURE PHENOMENA

The tensile strength of a brittle or glassy material was first shown by Griffith[5] to be inversely proportional to the square root of the flaw size, c, i.e.,

$$\sigma_c = \sqrt{\frac{2 E \gamma}{\pi c}} \tag{1}$$

where $\sigma_c$ is the critical tensile value required to cause the crack to propagate,

$E$ is Young's Modulus for the material,

$\gamma$ is the fracture surface energy per unit area of the crack surface, and

$c$ is the flaw size present in the material.

Now Equation (1) is based on the assumption that small cracks or flaws exist in the material. In most cases, microscopic flaws do exist in the material as a result of solidification or fabrication history. Even with extreme care in preparation, atomic size cracks can result when dislocations "pile up" at a barrier.[6] Since poly (methyl methacrylate), PMMA, the material examined in this work, is not crystalline, dislocation theory will not be discussed here. Dislocations should not be overlooked in fracture analysis of crystalline materials.

Griffith's Equation (1) uses Inglis'[7] mathematical solution for stress and strain energy in an initially cracked thin plate. The initial flaw length was assumed to be much longer than the plate

thickness. For a thick plate where c is not much larger than the plate thickness, Equation (1) is modified to

$$\sigma_c = \sqrt{\frac{2 E \gamma}{\pi c (1 - \nu^2)}} \tag{2}$$

where $\nu$ is Poisson's ratio of the material. Griffith verified that $\sigma$ is inversely proportional to $c^{1/2}$ by applying internal pressure to glass with microscopic flaws.

Orowan[8] and Irwin[9] later applied Griffith's principles to steel and found the measured value of $\gamma$ to be $10^3$ times larger than the theoretical surface energy value. They postulated that the large discrepancy is due to a plastically deformed layer near the crack tip absorbing a large amount of irreversible work during crack propagation. To account for this additional effect, Equation (1) becomes:

$$\sigma_c = \sqrt{\frac{2 E (\gamma + P)}{\pi c}} \tag{3}$$

where P is the work of plastic deformation. Orowan showed for steel, by X-ray diffraction studies, that $P >> \gamma$. $\gamma + P$ includes not only theoretical surface energy, but irreversible work, environmental influences on surface energy, crazing, and molecular orientation. Williams[10] proposed a qualitative expression for Equation (1), which includes these effects, i.e.

$$\sigma_c = k \sqrt{\frac{E (\gamma_b + \gamma_d + \gamma_v + \ldots}{2c}} \tag{4}$$

where k is a geometric constant while the subscripts b, d, v, . . . stand for the brittle, ductile, and viscoelastic dissipation processes, respectively. Note, $\gamma_d$ replaces P earlier mentioned. Equation (4) takes into account possible fracture mechanisms for a variety of materials. For a thorough review on fracture phenomena see reference (11).

### *2.1 FATIGUE FRACTURE*

Cyclic fatigue in materials is an important factor in determining the useful life of structures and machines. Glassy polymers, such as PMMA, are often analyzed with the classical fracture mechanics approach used for metals.[12] Fatigue failure in glassy polymers occurs due to crack initiation and propagation under moderate loadings. For a wide range of materials, i.e., metals, glassy polymers, and natural rubber, the following equation is found experimentally to hold

$$\frac{dc}{dN} = B\,\tau^n \tag{5}$$

where N is the number of stress cycles, c is the crack length, B and n are constants, and $\tau$ is a function of crack length and of temperature. For surface cracks, $\tau$ has the form of kcW where W is the stored energy and k is an undetermined constant. Assuming the existence of inherent flaws of maximum length $c_o$, Equation (5) can be integrated to predict fatigue life $N_f$ to give:

$$(B\,k^n\,W^n\,(n-1)\,c_o^{n-1})^{-1} = N_f \tag{6}$$

where $c_f$ (crack length at failure) is much greater than $c_o$ and $n$ is larger than 1. No actual predictions of fatigue data are available for PMMA used in this study but experimental data for natural rubber[13] and polyethylene support this theoretical approach for evaluating $N_f$.

# III. WAVES IN SOLIDS

In rigid body dynamics it is assumed that when a force is applied to any point on the body, the resultant stresses are uniform throughout the body. That is, the force is assumed to produce a linear acceleration into the whole body. In an isotropic elastic solid, this is not the case. Here, two types of elastic waves[15] may be produced; a dilatation wave which travels with a velocity

$$\left( \frac{K + (4/3)\mu}{\rho} \right)^{1/2} \tag{7}$$

and a distortional wave with a velocity

$$(\mu/\rho)^{1/2} \tag{8}$$

where k is a the bulk modulus, $\rho$ is the density, and $\mu$ is the shear modulus. In general, when an elastic solid is deformed, both dilatational and distortional waves are produced. In addition to these waves, a third, known as Rayleigh waves, may be propagated along the surface of a solid. The disturbances associated with Rayleigh waves decay exponentially with depth. This is of particular importance in seismic measurements but negligible in many other cases.[15]

Dilatational and distortional waves are altered during propagation through the solid. For instance, waves with periods close to the relaxation time of the media are severely damped. The wave energy may also be dissipated as thermal energy due to temperature gradients induced by wave motion. If there existed an ideal media

with no attentuation properties, an irregular dilatational wave front might eventually transform into a square front, provided that stress level were sufficiently high to reach non-linear behavior.

Shock waves are jump discontinuities in strain, stress, and in particle velocity in a material.[16] A non-square wave front with a very high stress may, after a period of time, transform into a square wave front. This depends primarily on a minimum amount of wave attenuation during propagation. Thus, a high stress dilatational wave, theoretically, may transform into a shock wave. Kolsky[15] defines shock waves as any wave produced by an instantaneous pressure pulse applied to a medium. It is questioned, however, whether shock waves do develope in materials[15,17] at other than stress levels in the kilobar (and higher) range.

Consider a plastic wave traveling in an elastic media with elastic properties up to a given stress. At stresses above the elastic limit, plastic flow occurs. Thus, an elastic wave would travel through the material with the plastic wave trailing at a lower velocity. Similarly, if the pressure pulse duration (necessary for shock) were long enough, a plastic wave could trail a shock wave. Generally, extremely short pressure pulses are required to produce shock waves, eliminating time needed for plastic wave formation. The material immediately in front of the shock front is taken from its original state to a greater density and a higher pressure in a single step. Without plastic wave formation, one should expect, even in ductile solids, a brittle

fracture from shock waves.

Now consider the stages when a plane compression pulse of arbitrary shape is reflected at a free surface, as shown in Figure 1. The resultant stress at any point in the media during reflection is obtained by adding the incident stress to the reflected pulses, designated by the thin line in Figure 1. The resultant stress is shown by the thickness line while the broken line refers to the reflected portion. This sequence of reflection covers the start, where only compression is present, to the finish where tension remains.

Similarly, a compressive shock wave will reflect from a free end to give a tensile shock wave, as shown in Figure 2. When the tensile component reaches some critical stress, $\sigma_c$, necessary for fracture, a segment will "spall" from the main body. If a "true" shock wave is present, the spalled piece is one half the length of the wave. Other waves produce spalling by a similar action. In the case of a shock wave, the fracture is perpendicular to the longitudinal axis, while in an undefined wave, the fracture surface resembles the wave front, i.e., curved with respect to the longitudinal axis.

Experimentally a shock wave is extremely difficult to introduce into a solid. Attempts are frequently made to simulate shock in solids to better understand structural failure due to shock waves produced in nuclear explosions.

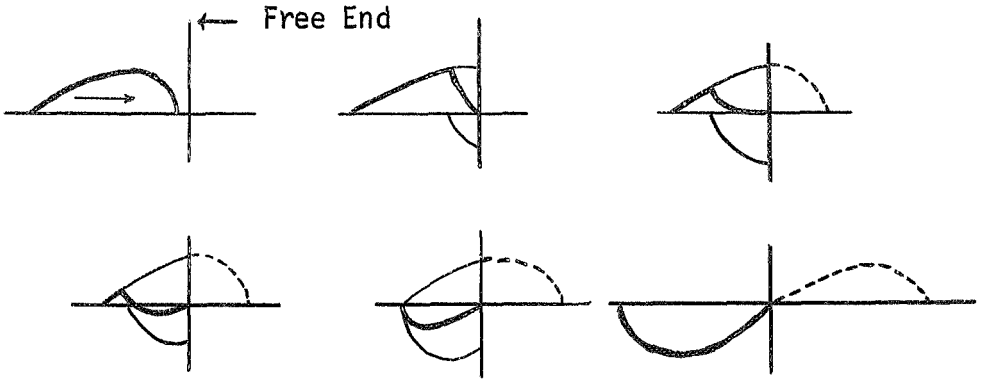


Figure 1. Reflection of irregular compression pulse at free end.

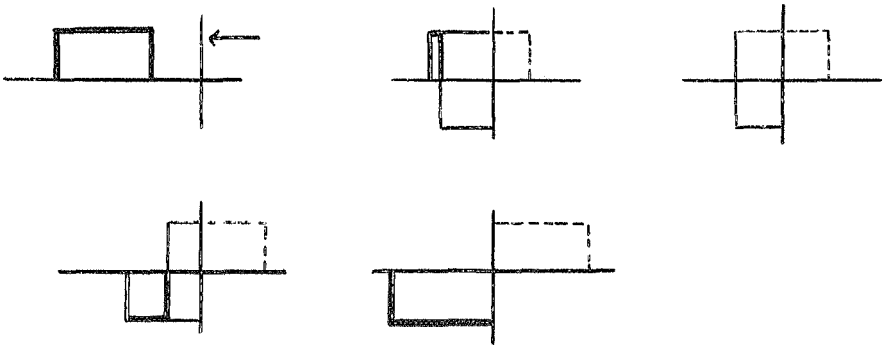

Figure 2. Reflection of square wave compression pulse at free end.

# IV. FRACTURE IN PMMA

According to the Griffith theory, the tensile strength of a brittle material is related directly to the surface energy but inversely related to the inherent flaw size, c, thus each influencing the material strength in opposite directions. Inherent flaws distort the stress field causing initiation of failure by extension of the largest flaw when a critical tensile stress is reached, as given in Equation (1). Surface energy is the energy required for the production of a unit area of fracture surface. The observed and the theoretical surface energy values for glass (a brittle material) are in good agreement as would be expected from the fracture surface examination. No plastic flow is present. In the fracture of steel, a considerable amount of plastic flow accompanies the fracture process causing energy dissipation. Consequently, the theoretical and calculated surface energy values differ by approximately $10^3$.[18] By comparison, the observed surface energy value for poly (methyl methacrylate), PMMA, is $3 \times 10^5$ ergs/cm$^2$ while the calculated surface energy value for C - C bond rupture gives 500 ergs/cm$^2$. This large discrepancy in the surface energy value for PMMA is attributed to the energy dissipated at the flaw tip.[19]

Microscopic examination of PMMA fracture surfaces produced at slow rates, i.e., uniaxial tension tests,[19] support a plastic deformation process.[18] As the crack propagates through the sample, there is a high tensile stress concentration at the tip of the crack. Because of this condition, the polymer molecules tend to

be drawn into an oriented configuration,[18,19] as illustrated in Figure 3. Color patterns present on fracture surfaces can be explained if this molecular orientation does occur. That is, the colors are caused by interference between light reflected from the surface and light reflected from the interface between the plastically deformed layer and the undeformed substrate. If the colors are due to optical interference, the difference in colors may arise from the differences in the thickness of the surface film. In support of this orientation layer hypothesis, Andrews[21] and Berry[22] observed a decay of color patterns with time and/or with an exposure to heat causing disorientation of polymer chains.

Fracture processes are reflected in the appearance of the fracture surfaces. Andrews,[21] Berry,[22], Zandman,[23], and Kies, et al.[24] describe PMMA fracture surfaces in degrees of roughness. Andrews classifies these degrees of roughness as mirror, mist, and hackle, as shown in Figure 4. Mirror refers to regions which reflect light specularly, mist denotes the area where no separate features are resolvable, and hackle is coarse roughness where fracture propagates on distinct different levels. When hackle is elongated in the direction of fracture propagation, the term "river markings" is often applied to it. The mirror region surrounds the fracture origin with an abrupt change into the mist region while hackle is found farthest from the fracture origin. All investigators are in agreement on the mirror region surrounding the fracture origin. Zandman[23] and Kies, et al.[24] have observed concentric ribs covered with closely packed hyperbolic figures en-

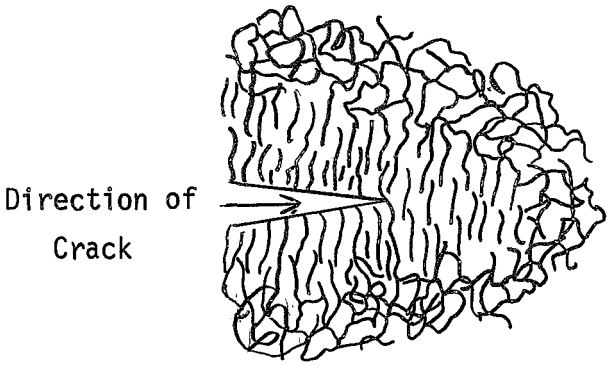


Figure 3. Proposed mechanism of molecular orientation during fracture in PMMA[17].

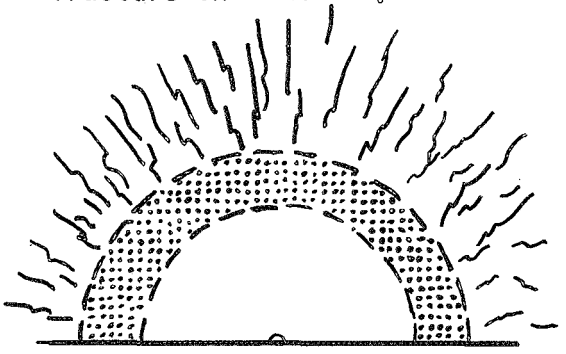

Figure 4. Proposed fracture surface in PMMA showing ( inside to outside ) fracture origin, mirror, mist, and hackle[18].

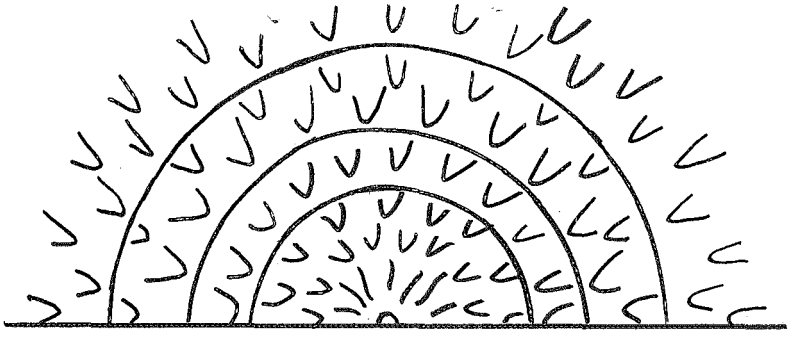

Figure 5. Proposed fracture surface in PMMA showing "ribs"[23].

closing the mirror area, as shown in Figure 5. Their tests revealed that these circular ribs are strongly dependent on the rate of load. Kies, et al. observed PMMA fracture resembling a brittle fracture mode at high rates of loading due to many flaws becoming active. Schardin[25] and Andrews[21] both measured for PMMA a crack velocity increase with increasing distance from the origin. As would be expected, the crack velocity and fracture surface are dependent on the loading history of the specimen.

The level differences within the PMMA fracture surface are often called tear lines or lag lines which represent boundaries between fracture elements propagating on different levels.[18] These level differences tend to produce a rough surface as compared to the mirror region. Postulating the energy absorption characteristics as the crack propagates through the specimen, the mirror region suggests little energy required as compared to the rough regions. That is, the tear lines associated with the rough areas represent a higher toughness indicating a greater energy required for crack propagation than in the mirror region.

Solid PMMA rods have internal flaws, i.e., voids, craze matter, or inclusions, as do most materials. These inherent flaws are recognized in PMMA as approximately 0.002" in diameter.[26,27] With reference to Griffith crack criteria, these flaws are initiation sites for failure with some applied critical stress. Thus, fracture occurs at some related stress given in Equation (1) for a corresponding flaw size.

A brief description of craze matter is necessary to understand

that crazes are a flaw source present in some thermoplastic materials. Crazing is encountered in a variety of commercial materials, i.e., polystyrene, polycarbonate, styrene-acrylonitrile copolymer, and PMMA. Considering PMMA exclusively, craze matter is an optical deterioration of the PMMA matrix,[18] which possibly results from the formation of cracks that impair light transmission causing optical aberrations. Crazing is attributed to residual stresses produced in forming operations, exposure to solvents, and applied tensile and flexural stresses.[28] Under tensile stresses, crazes appear normal to the load direction. These crazes reduce the strength of the material though the reduction is less than would be predicted for a true crack in the material. Kambour[29,30] defines craze matter in PMMA containing 40% void content. Kambour produced small, thin crazes in cast sheets of PMMA under dry conditions. Total light reflection of the crazes was observed to be a gradual process occurring over several degrees. Reflection began at approximately 44° incident angle on the bar surface with optimum reflection at 55°. Crazes in PMMA are a constant source for fracture initiation.

Postulating the effect of crack propagation of fracture surface roughness when a sharp reflected high energy tensile wave reaches a critical value for an existing flaw, a colorless surface should result. High tensile rates prevent the formation of plastic deformation, as observed by Keis, et al.[24] suggesting a colorless fracture surface. Surface fracture features (degrees of roughness) should resemble that proposed by Zandman[23] for matrix inhomogeneity

induced fracture under high tensile load rates. Surrounding these distinct fracture regions, a rough surface area should exist due to rapid crack propagation with subsequent catastrophic fracture (spalling).

# V. TEST APPARATUS AND PROCEDURE

As the title suggests, an exploratory effort was made to ascertain if a cumulative shock driven device is feasible on a small scale and if there are any measureable effects produced by cumulative shock loadings in a solid. Initial thinking in this area was on metal fracture, i.e., spalling. In view of the high energies needed and the surface deformation associated with each load, metal specimens seemed impractical.

At that point it was decided to examine polymeric materials under high stress rates. Polymers have one advantage over metals, that is, broken bonds (if sufficient in number) are detectable by electron paramagnetic resonance (EPR).[31] A Varian E 3 Spectrometer with regulated temperature control unit was used to investigate this effect. The initial experiments were on nylon 66 rods ranging from 0.030" to 0.050" in diameter. These specimens were furnished by the Plastics Department, E. I. DuPont de Nemours and Company, Inc. H. Kolsky[15] describes a simple apparatus for examining the propagation of waves in a wire shown in Figure 6. Here the end of a wire, W, is attached to a rigid member A with B, a vertical support rod fitting loosely into the tubular part of A. H is any weight which falls between two vertical rails after being accelerated by pre-stretched rubber bands. When H strikes A, the wire is stretched until the disk on A reaches the rod B. The circular notch at N on A breaks off when A has traveled the distance D and is stopped by B with the weight continuing downward. This design has two variables:

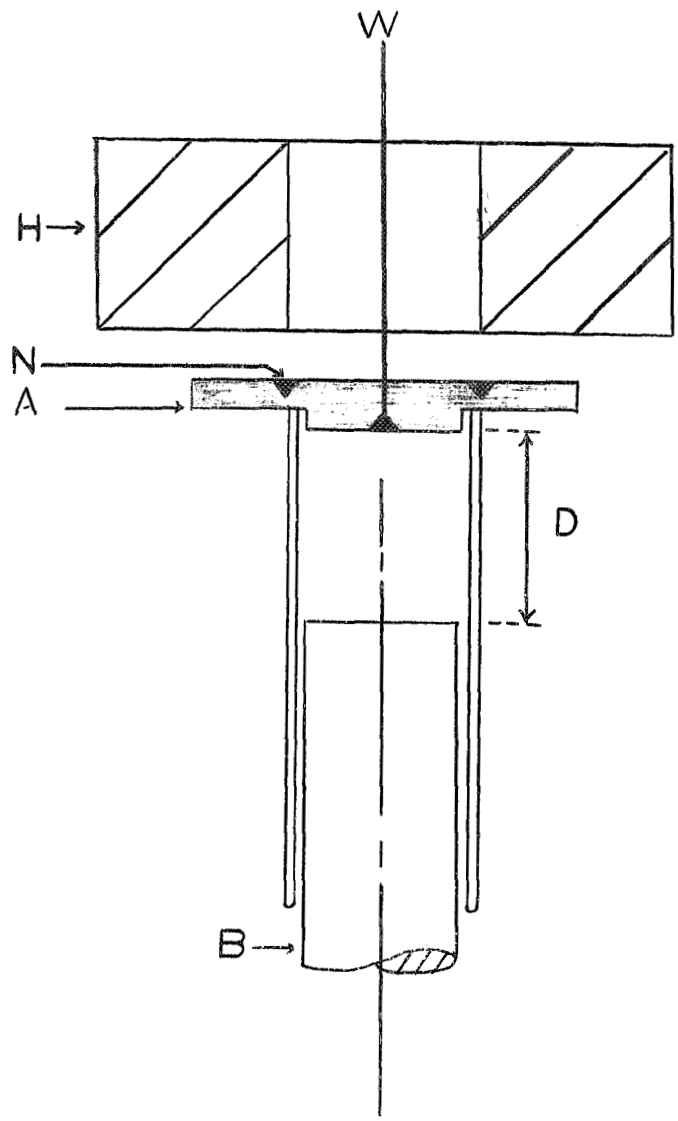


Figure 6. Schematic of apparatus for investigating the propagation of plastic waves in a wire.

time of impact controlled by changing D and the impact velocity governed by the pre-stretched rubber bands.

The device shown in Figure 6 was modified to accomodate repeated loading by replacing the notch, N, with a flat surface. Varying loads, H, were physically lifted and allowed to free-fall a predetermined height until intermediate specimen examination or specimen fracture. Drawn nylon rods were substituted for the wire specimen shown in Figure 6, due to availability and lower tensile properties than in wires. A standard grip was designed and made with complimentary parts, as shown in Figure 7. It was not clear whether the specimen fractured due to stress load or due to the gripping mechanism. With grip integrity doubtful, the alignment of the weight with each load critical, and the unpredictable rebound of the weight on impact, a new design was sought.

The next attempt to produce high tensile waves made use of a pendulum principle. A schematic of the test apparatus is shown in Figure 8. The object in this design was to allow the pendulum to free-fall a designated height, or through some angle $\theta$, similar to the Charpy Impact Tester.[24] Impact by the pendulum produced a compressive wave into the specimen. Here PMMA rods were used in place of nylon due to stiffness and easy machinability. Fracture should occur when the reflected tensile wave reaches some critical value $\sigma_c$, for some internal flaw. In this test apparatus, specimen holders were broken without any visible specimen damage. Since this was not the goal, this design was abandoned. It should be noted here that specimen holder failure was due to bending stresses

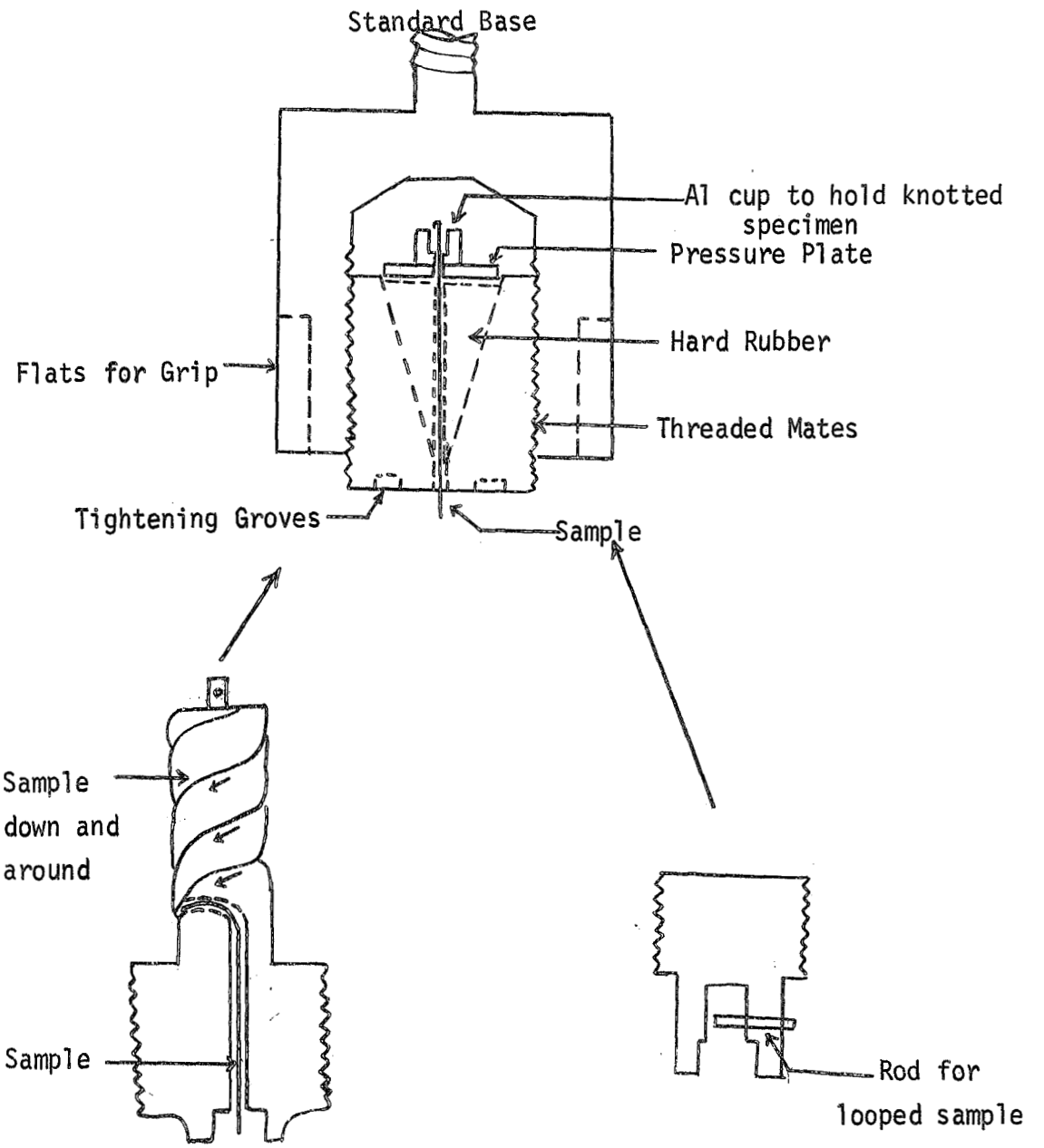


Figure 7. Sketch of standard gripper base with complimentary parts.

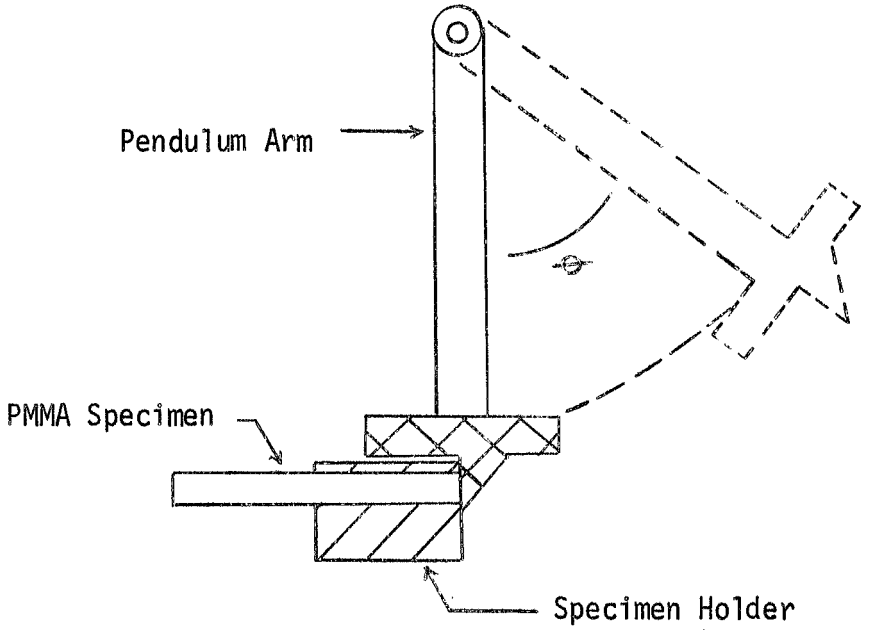


Figure 8. Sketch of Pendulum impact device with variable mass ( cross-hatched ) hammer.

rather than reflective tensile waves. The fractured surface resembled controlled metal bending fracture surfaces,[32] thus a detailed analysis of the fracture mode in the holder did not seem critical to this work.

With PMMA rods retained as the prime test material, a ballistic impact device was designed. A cylindrical steel chamber was built to accomodate firings from a .22 Colt revolver with interchangeable cylinders to accept 22 magnum cartridges. The standard cylinder plus the magnum cylinder allowed use of the following commercially available bullets:

Table 1.

BULLET VELOCITIES AND ENERGIES

| Bullet Name | Muzzle Velocity | Muzzle Energy |
|---|---|---|
| 22 C. B. Caps | Not known | Not Known |
| 22 Short | 1125 ft/sec | 81 ft. lbs. |
| 22 Long Rifle | 1335 ft/sec | 158 ft. lbs. |
| 22 Winchester Magnum Rim Fire--Full Metal Case | 2000 ft/sec | 355 ft. lbs. |
| 22 W.R.F. Remington Spl. | 1450 ft/sec | 210 ft. lbs. |

These bullets were selected because of their range of muzzle velocities and muzzle energies. The above list does not represent all bullet loadings available for this caliber. Figure 9 shows the complete test apparatus while the critical section of the apparatus, the piston and specimen chamber, is shown in more detail in Figure 10. The

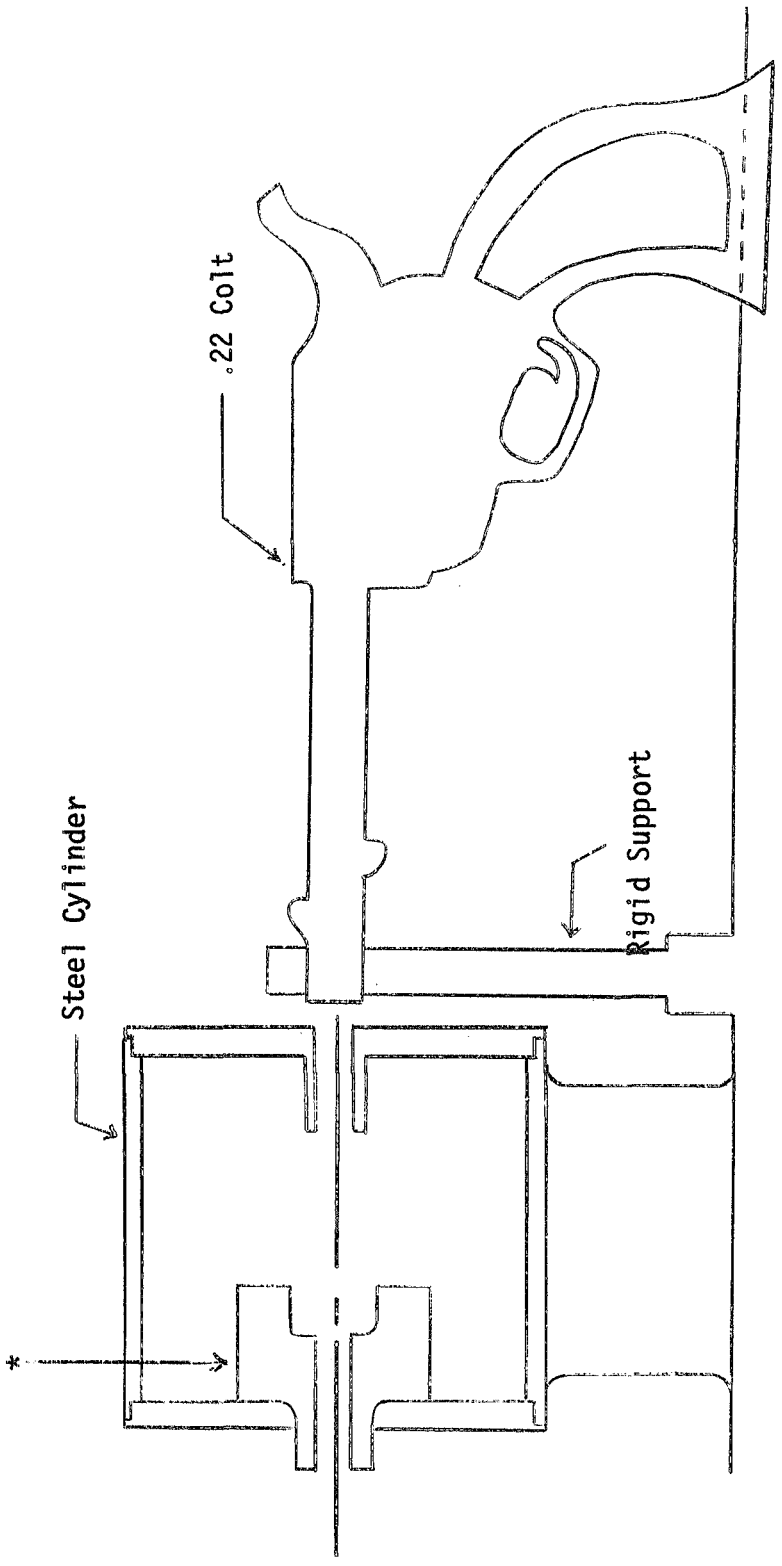


Figure 9. Schematic of ballistic loading device, * shown in more detail in Figure 10.

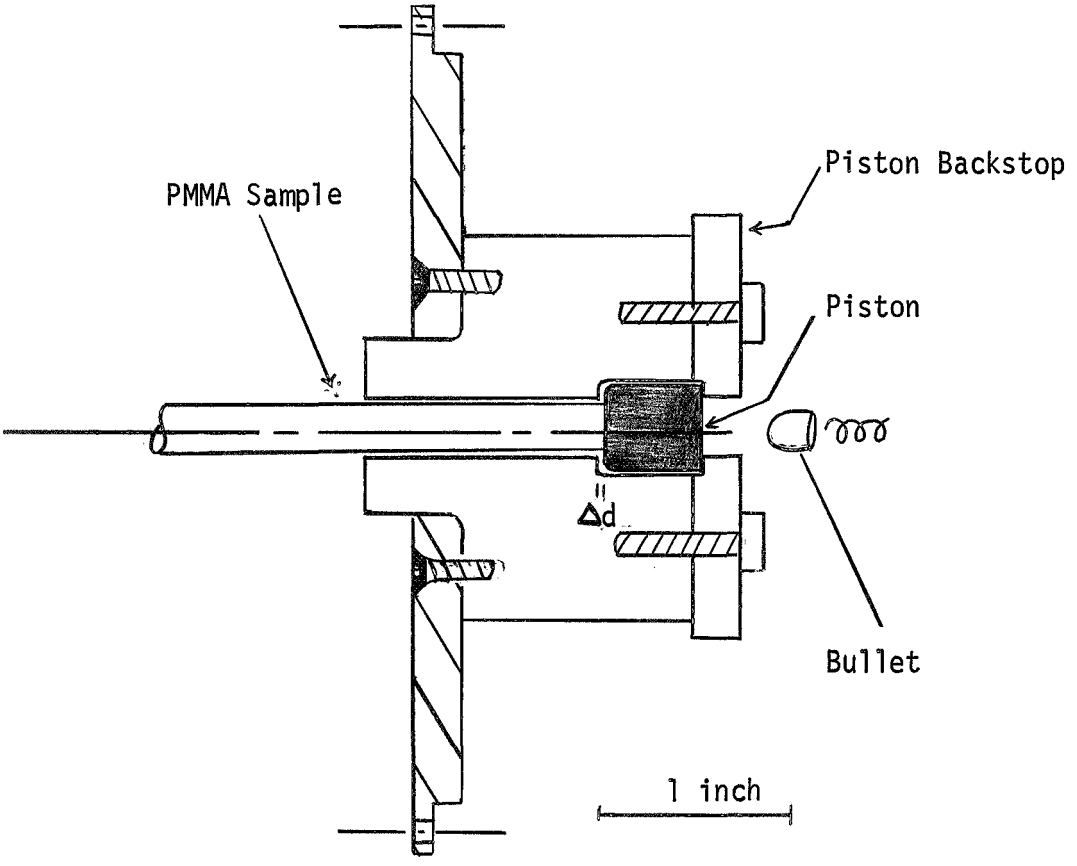


Figure 10. Piston and specimen section of ballistic impact design: ( drawn to scale ).

specimen holder and the piston were machined from 4140 steel and hardened to 50 Rockwell Hardness in an inert atmosphere. Care was taken to avoid sharp corners in the heat treated parts. Cleaning, i.e., sand blasting, was avoided to minimize internal stresses.

PMMA rod ends were cut flat and polished smooth with 600 grit polishing paper. Silicone vacuum grease was used as a wetting agent to insure good wave transfer from piston to specimen. Once the gun was fired, the bullet impacted the piston which initiated a large compression wave in the PMMA rod. The wave amplitude (stress) was governed by the bullet loading, i.e., high muzzle energy bullets produced wave intensities larger than low muzzle energy bullets. The time of impact was regulated by the position of the piston backstops, i.e., $\Delta d$. After impact, the piston rebounded with a large force into the piston backstops.

The introduced stress wave was examined by bonding the barium titanate piezeolectric crystals on the PMMA rod using Eastman 910 Epoxy cement. The crystal transducer leads were connected to a Tetronix Type 556 Dual-Beam oscilloscope set at 50 $\mu$ sec/cm scan rate. Figure 11 shows the oscilloscope trace as the wave traveled by the transducer. A similar transducer on the outside diameter of the piston chamber was used to trigger the oscilloscope. A detailed wave description cannot be obtained with these transducers since they are non-uniform sizes. Since these transducers are positioned on the outside of the rod, they respond to dilatational, distortional, and Rayleigh wave components. To obtain a complete description of the wave, crystals with physical

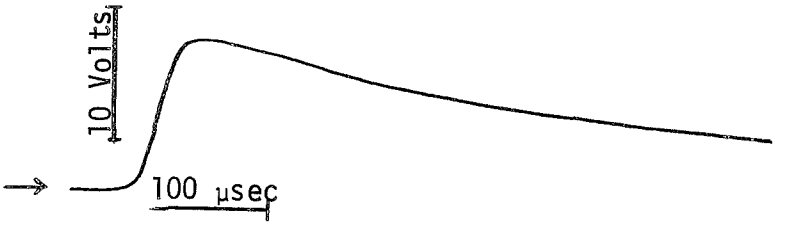


Figure 11. Typical oscilloscope trace showing wave shape as it travels through the PMMA rod.

properties similar to PMMA should be sandwiched into the rod. This would then only give the shape and length of the dilatational wave component. More sophisticated techniques of monitoring waves are available,[3] but none quite as simple as the one described.

To obtain a better understanding of the fracture phenomena, i.e., spalling, a 16 mm camera (HYCAM 1004 E-115) was used to photograph the fracture sequence: starting of rod movement, fracture 0.5" from the rod end, and separation of the sections. The fracture description plus enlargements of the critical frames are discussed in the PMMA Fracture Examination.

# VI. DISCUSSION OF TESTS

## *6.1 PMMA EPR EXAMINATION*

Attemps were made to obtain some measure of internal damage produced during ballistic impact loading of PMMA rods. EPR spectroscopy is a suitable technique for monitoring covalent bond rupture in polymers. A 1/4" drawn PMMA rod, commercial grade purchased at Plastic Products Company of Utah, Salt Lake City, was examined for a residual EPR signal. Figure 12 shows a typical residual spectra for the rod at - 150°C. Low temperatures are used to enhance any signal[31] which might be present. To see the effect, if any, from ballistic impact loading, two rods were immediately examined after impact. The rods were quenched in a liquid nitrogen bath to preserve any damage introduced during impact. Neither of the specimens were fractured during impact. Figure 13 shows a representative spectra of the loaded rods. There was not a noticeable difference between the residual spectra and the test spectra. From this undefineable spectra, it was apparent that not enough damage was produced under this condition to be detected by the EPR spectrometer.

## *6.2 PMMA FRACTURE EXAMINATION*

A 1/4" diameter, commercial grade PMMA, was ballistically loaded with a wide variety of test conditions. Short rods, long rods, pointed rods, machined grooved rods, and annealed rods were examined. In addition to varying the rod dimensions, different bullet

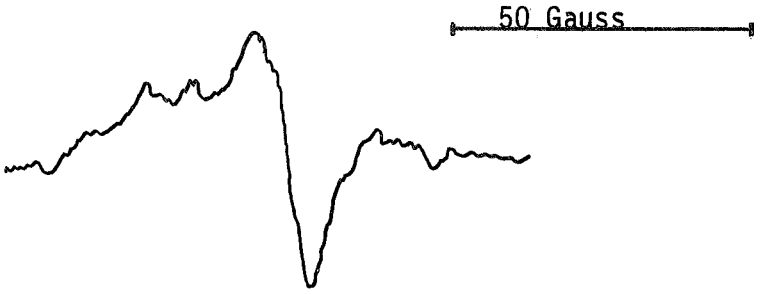


Figure 12. Free radical spectra of residual signal in 0.250 in. diameter rod at -150°C and at a gain of $3 \times 10^6$.

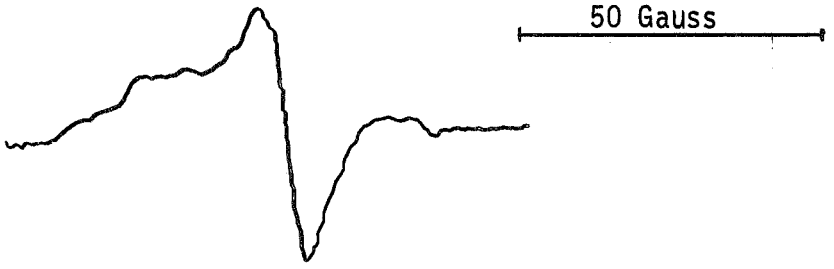


Figure 13. Free radical spectra of 0.250 in. diameter PMMA rod ballistically impact loaded: recorded at -150°C and a gain of $3 \times 10^6$.

loadings (shown in Table 1), a range of piston masses* and varying piston travel distances** were used. The number of variables associated with the ballistic loading design, shown in Figure 9, provides for a number of tests to produce fracture immediately or after several loadings. Table 2 summarizes the test parameters with respect to rod dimensions.

TABLE 2

SPECIMEN DIMENSIONS TESTED

| | Rod Length | Free end Shape | Observations |
|---|---|---|---|
| 1. | > 4" | flat | Uncontrollable failure, microscopic examination indicated fracture due to bending stresses |
| 2. | < 4" | flat | Quite predictable, fracture initiates from voids or inclusions |
| 3. | > 4" | pointed | Same as 1 without noticeable difference |
| 4. | < 4" | pointed | Same as 2 without noticeable difference |
| 5. | Annealed different shapes and lengths | | No difference from as-received rods |
| 6. | Grooved notches on various lengths with flat ends | | Fracture at groove position when the groove is placed passed the overlap of the tensile and compressive components. Loads less than needed for failure in a whole rod produced fracture everytime. |

*Constant piston masses were used for all these tests.

**Piston travel distance was kept constant (0.040").

A brief description is necessary at this point to describe the problems associated with commercially available PMMA. A six foot length of 1/4" drawn rod had a diameter which varied from 0.250" to 0.290". This limited the specimens used in that the specimen chamber would not accept diameters larger than 0.270". In addition to the variable rod diameter, small black inclusions, approximately 0.0044" large were scattered throughout the rod. These inclusions appeared on the average, one for every six inches of rod. Since the scope of this study was to develop a test apparatus capable of introducing high stress waves into materials, quality controlled PMMA rods were not used.

As mentioned earlier, Table 2 lists the various sample geometries tested with particular results for each type. Since fracture was more easily controlled on samples less than 4" long with flattened ends, the remainder of the discussion will deal with this geometry. To accomodate some variance in rod diameter, 0.020" oversize boring of the specimen chamber was performed before heat treatment with subsequent tempering to 50 Rockwell. Rod diameters less than the oversized chamber, very near 0.250", were symmetrically positioned in the chamber by placing 1/8" wide strips of Scotch mending tape near the rod impact and 1/8" from the chamber outlet. In some cases two complete tape windings were needed while in others only one. With the sample aligned, bending upon impact was avoided.

Before each individual test, the rod was examined for inclusions with respect to the impact end. After fracture the pieces were re-examined with respect to these inclusions. In general, four

distinct modes of fracture were observed: 1) "solo fracture disks" with inherent flaws, i.e., voids or craze matter, 2) "fracture disks" with inclusions at the origin and cyclic rings surrounding it, 3) surface fracture disks (inclusion initiated) with cyclic rings, and 4) bending fracture. These four fracture morphologies are common to all ballistically loaded rods less than 4" long. Each feature will be discussed and illustrated individually:

1) Solo Fracture Disks

Approximately 30% of the fracture surfaces examined resembled the flaw region shown in Figure 14. The clear, flat, shiny, semi-circular area will be referred to as fracture disks. These fracture disks resemble "craze matter" observed by Kambour[29,30] at incident angles between 44° and 55° in PMMA sheets. Careful examination of the rod, between loadings and before fracture revealed these "crazes" normal to the longitudinal axis. With each additional load, the number of these crazes increased. By recording their location with respect to the impact end, fracture did occur in a plane containing these sites or site.

In Figure 14 the fracture disk represents the fracture origin with the center acting as an inherent flaw, mentioned earlier.[24,25] Optical measurements of these observed inherent flaws vary from 0.0008" to 0.002" in diameter depending upon individual fracture disks. The outer diameter of the fracture disk varies from 0.003" to 0.03".

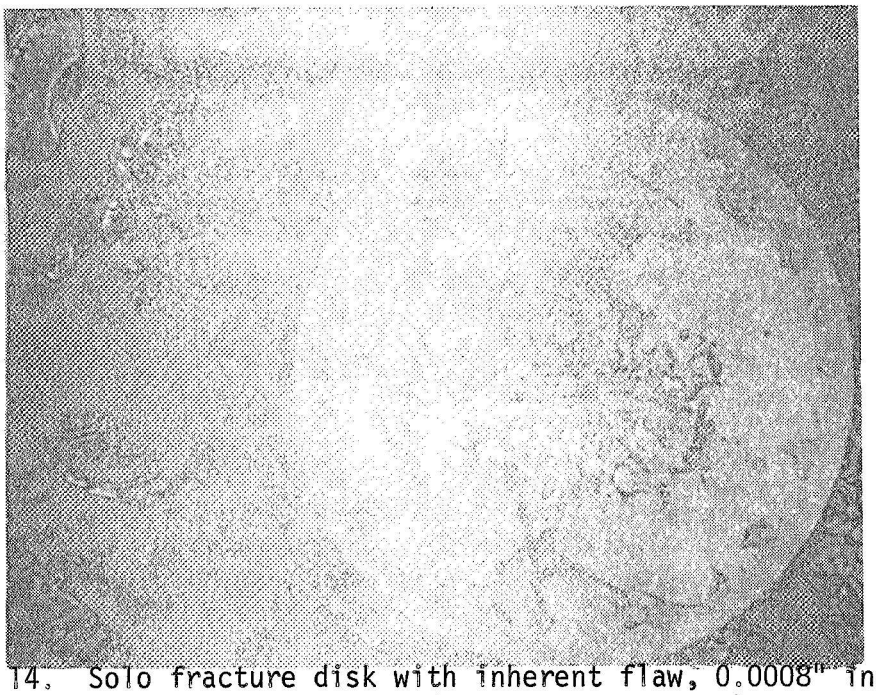

Figure 14. Solo fracture disk with inherent flaw, 0.0008" in diameter: 100X (Optical Microscope).

Figure 15. Solo fracture disk obscured by overlay and chipping out during fracture: 50X (Optical Microscope).

Figure 15 is a lower magnification optical photograph of the area surrounding and including Figure 14. Here, segments of fracture disks appear to overlap one another, while in fact, these segments are on different levels with portions chipped out. The small pieces that chipped out were recoverable, but extremely crumbly, making microscopic examination impossible.

The degree of surface roughness, with respect to mirror, mist, and hackle, as shown in Figure 4, includes the mirror only, in this fracture mode. Kies, et al.[24] observed PMMA fracture resembling a brittle fracture at high rates of loading due to many flaws becoming active. The area shown in Figure 15 includes several fracture disks suggesting a similar fracture mechanism.

2) Fracture Disk with Cyclic Rings

This particular pattern, as shown in Figure 16, occurred in 40% of the fracture surfaces examined. This fracture surface initiated at an inclusion in the bulk of the specimen with a cyclic ring or "rib"[23] surrounding the fracture disk. The sharpness of the cyclic ring (rib) indicates a high rate of loading as observed by Zandman.[23] Zandman's tests used uniaxial tension to produce fracture as opposed to reflected tensile wave components used in the author's work. Even though the surfaces are very similar, the rib observed in Figure 16 suggests cyclic loading. Since a single load produced fracture, a feasible explanation for

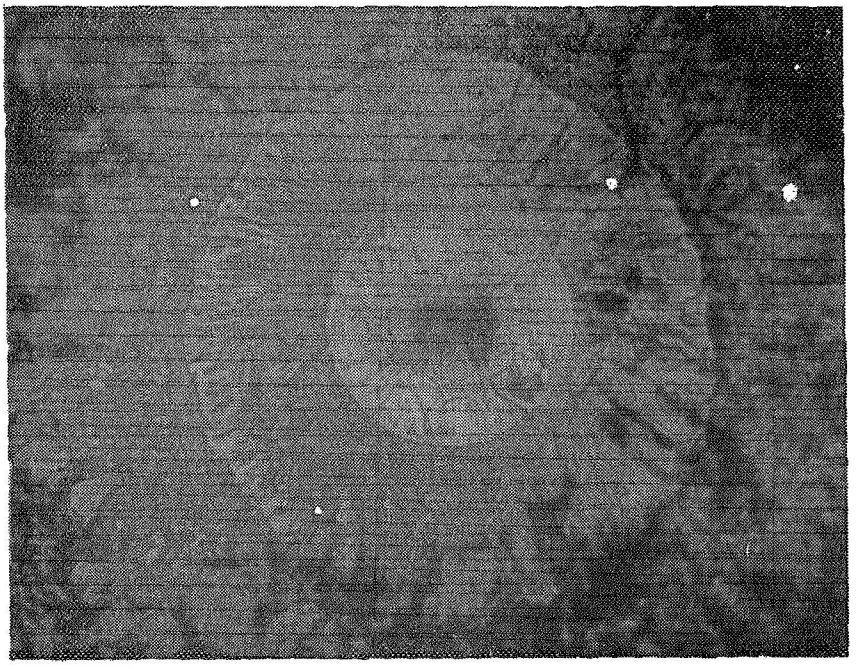

Figure 16. A fracture disk inclusion initiated with one cyclic ring in a PMMA fracture surface: 100X (Optical Microscope).

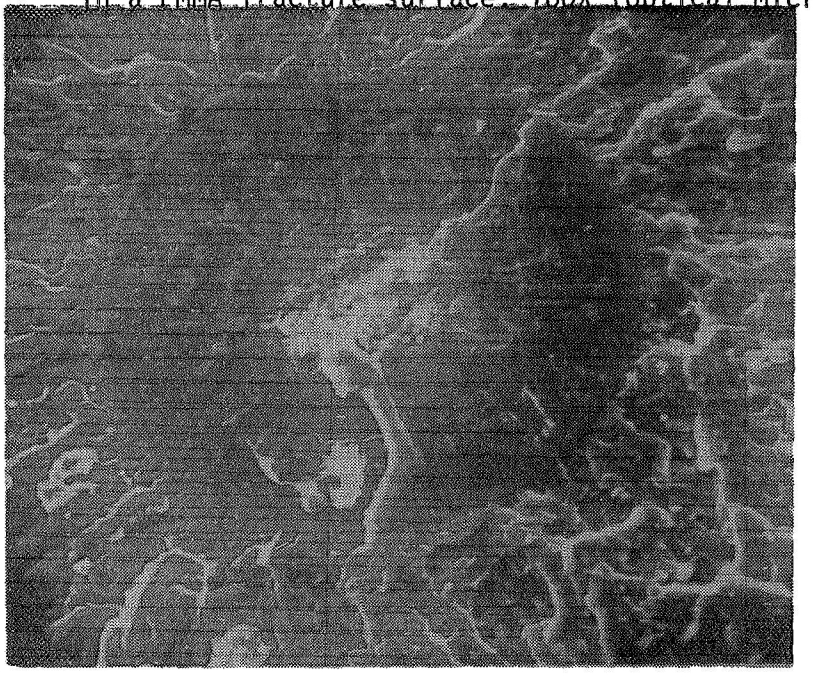

Figure 17. Same area as Figure 16 examined with a Cambridge Scanning Electron Microscope: 260X.

this apparent phenomena is to consider the wave traveling back and forth through the rod. Each pass of the reflected tensile wave component increases the crack (craze matter) diameter as long as the stress is above $\sigma_c$. Once a critical flaw size is reached, catastrophic failure follows. This appears to be a reasonable explanation for the existence of the ring but the question arises then: Why does it appear in uniaxial tensions tests?[23] This particular fracture disk morphology is not limited to one cycle or rib as shown here. Additional rings surrounding the initial fracture area, mirror, are present in some main fracture surfaces as well as in surface flaw initiation, described in the third mode.

A scanning electron micrograph, Figure 17, shows the various levels of the flaw area. Figure 18 is a low magnification scanning electron micrograph to illustrate the drastic difference between the matrix and the fracture disk area.

3) Surface Flaw Initiation

Approximately 30% of the rods failed due to surface flaw initiation. As shown in Figure 19, fracture disks with corresponding cyclic rings exhibited two modes of fracture initiation. Figure 19-a has small, approximately 0.0005" in diameter, spherical inclusions on the surface and in 0.0015" deep. These small inclusions do not appear to have any significant effect on the fracture

Figure 18. Representative low magnification scanning electron micrograph of Figure 17: 26X.

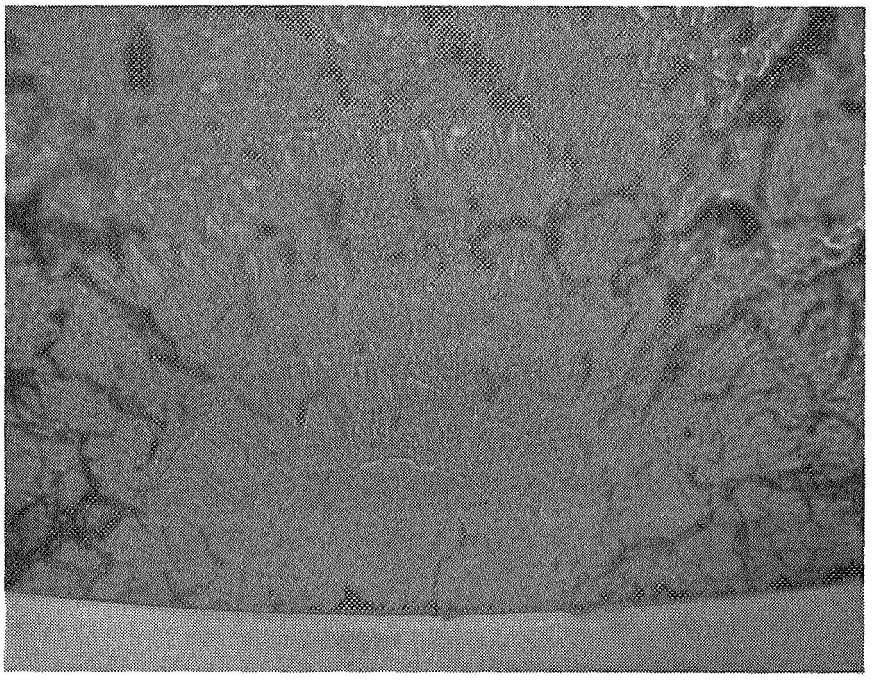

Figure 19(a). Surface flaw fracture disk initiation from inclusions approximately 0.0005" in diameter: 100X (optical microscope).

Figure 19(b). Surface flaw fracture disk initiation from inclusions approximately 0.006" in diameter: 100X (optical microscope).

disk pattern as in Figure 19-b. Here, large (approximately 0.006" in diameter) inclusions in 0.01" deep alter the fracture disk cyclic rings and obscure the origin. Even though both surface flaws have cyclic rings, the rings associated with the small inclusions are more regular and distinct than those surrounding the large inclusions. In general, there exists not more than two such patterns per fracture surface. This particular fracture initiation demonstrated the significance of surface conditions in studying fracture. The individual regions shown here, as described by Zandman, are identical to those described in failure mode 2.

4) Bending Fracture

This type is not included in the percentage of controlled failures. Bending fracture morphology as observed in metals[32] approximates the surfaces observed in PMMA. These fractures occurred when the rod was not aligned within the specimen chamber and/or the rod was not flat against the piston. These surfaces were not examined microscopically.

These three fracture morphologies represent the fracture surfaces produced when loaded once or several times to failure. No marked difference was observed in the fracture when loaded with a 22 long rifle or Magnum cartridge. The number of rings surrounding the fracture disks did not correspond to the number of impact loadings. Due to rod irregularities, cumulative loading to failure was not predictable. Quality controlled rods should be examined under

repeated loadings to determine cyclic rate as a function of number of cycles to failure.

The fracture sequence was recorded with a 16 mm camera to determine when fracture occurred and if the rod bent or twisted after impact. A 3" long rod was impact loaded with a 22 Winchester Magnum Rim Fire (Full Metal Case) once to produce failure. Figure 20 shows the fracture sequence, while Figure 21 is a schematic of the rod after fracture. One hundred feet of Tri-X film recorded the fracture sequence at 8,000 frames/sec. The enlargements of the critical frames shows the various pieces spalling off the end. This particular rod had no inclusions in its matrix. Microscopic examination of each fracture surface positively identified the sequence of pieces, that is: (1) is a mate to (2), (3) is a mate to (4), and (5) is a mate to (6). Distinct fracture disks as shown in Figure 14 identify surfaces (1) and (2). Figure 22 shows two large fracture disks with a smaller one as found on surfaces (3) and (4). Surfaces (5) and (6) were initiated by surface flaws similar to Figure 19-a. This one fractured rod included two of the three fracture morphologies observed throughout the tests. Since no inclusions were present in the rod, fracture associated with inclusions could not be expected.

This segment of the examination established the direction of the rod after impact, the approximate time of fracture, and the variety of fracture morphologies contained in one fractured rod.

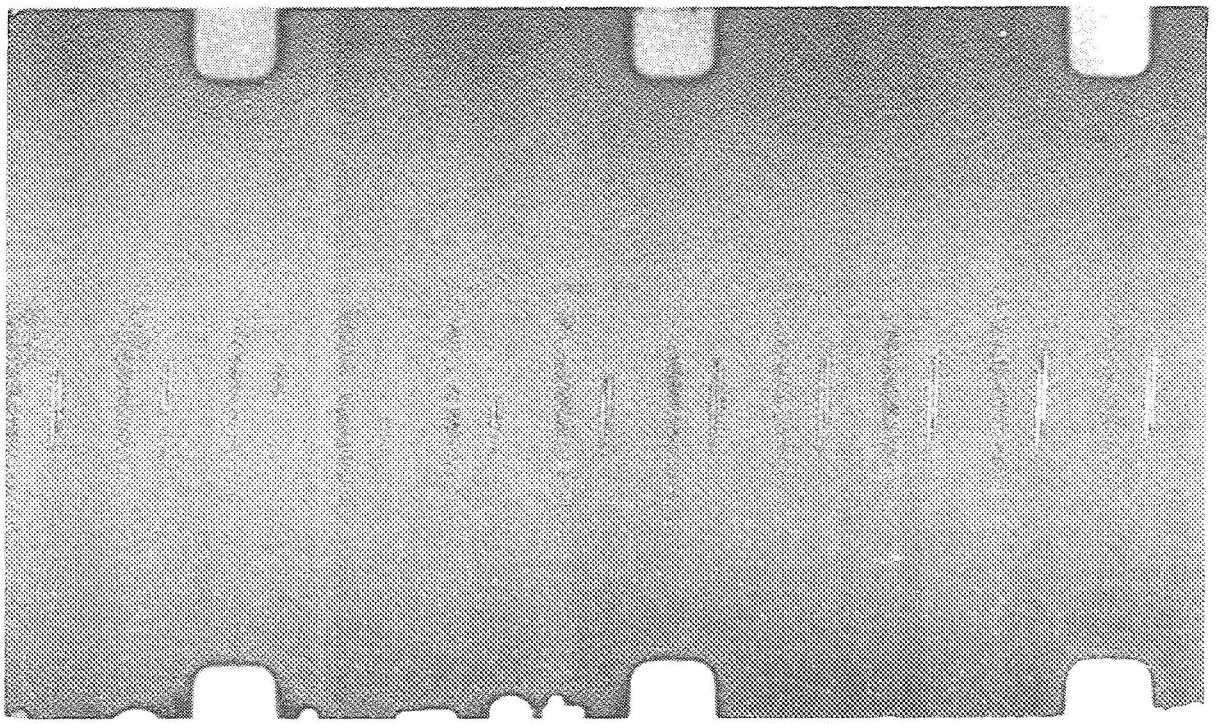

Figure 20. Fracture sequence at 8,000 frames/sec. (left to right): 1) rod intack, 2) spall initiation at surfaces (5) and (6) as shown in Figure 21, 3) spall initiation at surfaces (3) and (4), and 3) complete separation of spall pieces.

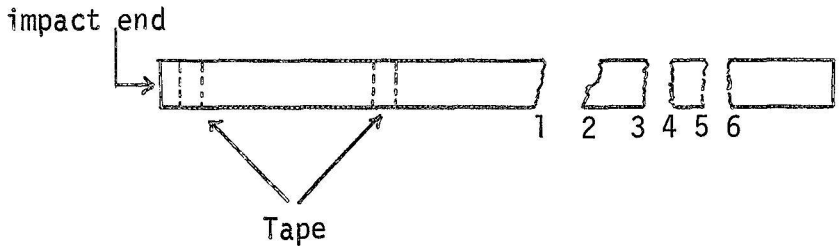


Figure 21. Schematic of spalled PMMA rod used for photographing fracture sequence: ( Drawn to scale ).

Figure 22. Solo fracture disks as found on rod photographed with a 16 mm camera: 50X (Optical Microscope).

*6.3 CUMULATIVE LOADING IN PMMA*

By using the ballistic impact loading apparatus, as shown in Figure 9, cumulative loading in PMMA rods were possible with a minimum time delay of 5 sec between firings. The 22-Colt revolver accomodated a range of bullet loadings, as shown in Table 1, capable of producing specimen failure with one or several impacts. Rods less than 4" long were the easiest to fracture as discussed earlier. Due to the PMMA irregularities, cumulative loading was impossible to control. For example, rods (visibly identical) subjected to the same load histories behaved differently. The rods would either fail after one load or after repeated loadings with six loads being the maximum. Often, but not always, craze disks would appear within the rod during the loading cycle to act as fracture initiation sites. Cartridges having muzzle energies less than the 22 long rifle never produced fracture with one load or with any definite number. Cartridges having muzzle energies greater than the 22 long rifle produced fracture with one impact. These larger bullets caused more than one slice to spall off the rod end with one firing. With fracture produced repeatedly with one loading, cumulative damage was impossible with these cartridges. To guarantee failure when photographing the fracture sequence, these larger loadings were used.

As far as can be determined from the tests, the variance in failure conditions is caused by the PMMA irregularities and not the test apparatus. No possible reason is evident at this time to suspect unreliability in the test apparatus.

*6.4 OTHER MATERIALS TESTED*

A 1/4" diameter urethane rod*** was ballistically loaded to failure. To help reduce the critical stress necessary to cause fracture, a knife cut was made around the circumference, approximately 2/3 of the radius deep. Both ends of the rod were cut flat to give a uniform specimen geometry. The rod was placed in the specimen holder and loaded once with a 22 long rifle bullet. Optical examination of the rod at this point showed no visible damage. The rod was remounted and impact loaded this time with a 22 (hollow point) Winchester Magnum Rim Fire bullet. This larger loading produced failure, i.e., spalling, at the reduced cross-sectional area made by the knife cut. Microscopic examination of the center of the fracture surface revealed an intricate fracture zone shown in Figure 23. Lettering on the composite photograph denotes the fracture history. High magnifications, i.e., above 100x were impossible to focus with the Unitron due to sharp steps and falls in the surface. The lowest magnification, 50x, showed the most detail. A closer look at the fracture pattern with a Scanning Electron Microscope is shown in Figure 24. The crack formation of the 0.4" fracture ring initiates at the knife cut interface. The crack formation resembles "river patterns"[21] found in cleavage failures of most metals, in that the number of "tributaries" decreases in the direction of crack propagation.

An optical grade, non-annealed, 1/4" glass rod was impact

---

***Furnished by N.A.S.A. Grant NGR 45-003-029.

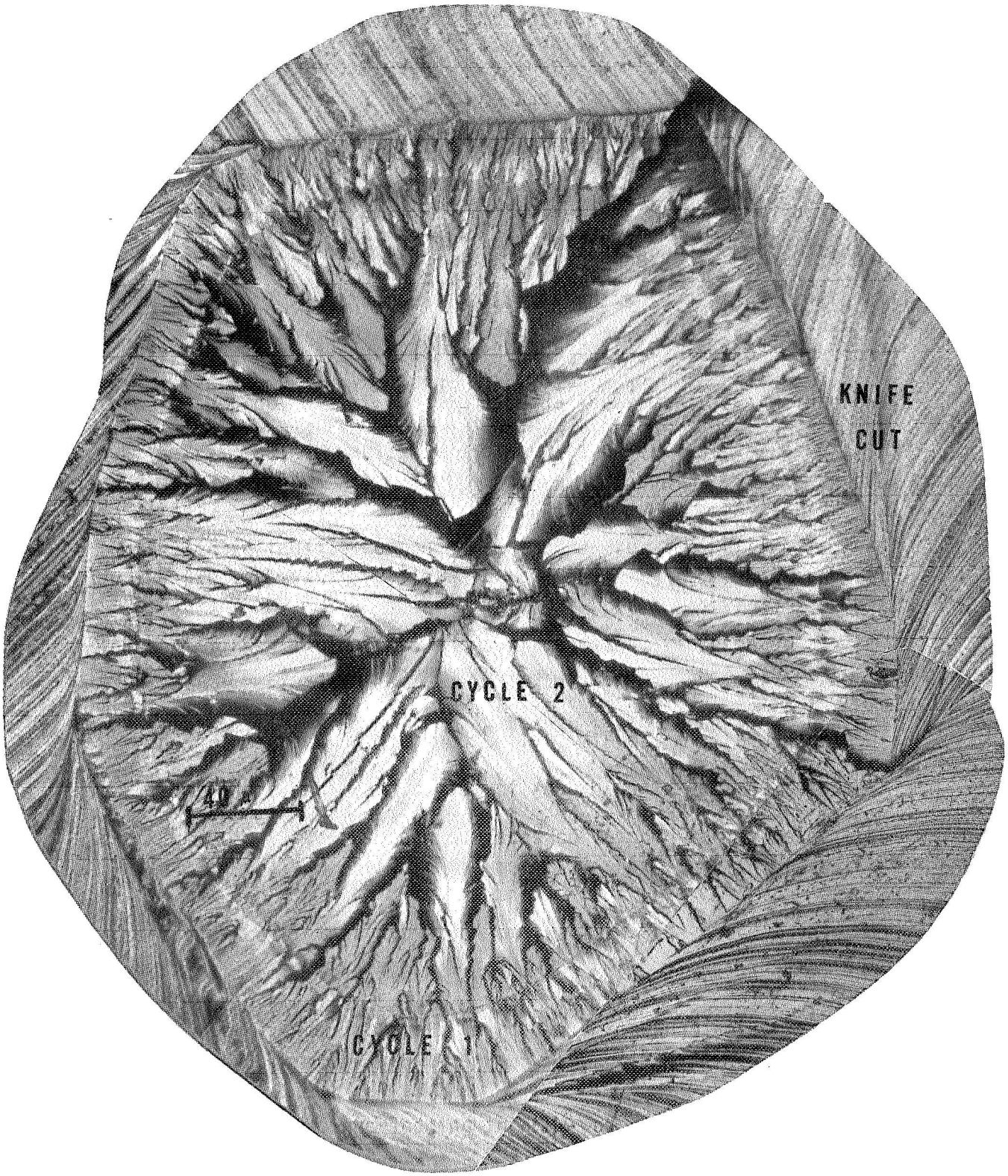


Figure 23. Cumulative fatigue damage in a poly-urethane 1/4" daimeter rod: 50X (Optical Microscope).

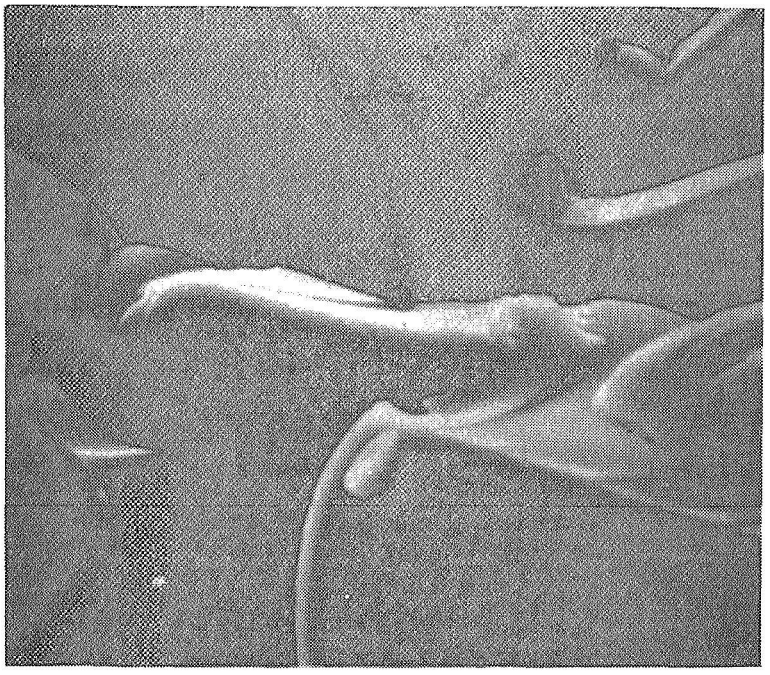

Figure 24. Electron micrograph showing the different levels associated with cracks in Figure 23: 500X (Cambridge Scanning Electron Microscope).

loaded with a 22 C.B. Cap (muzzle energy and muzzle velocity less than a 22 short) once for fracture. Powdery to two inch long pieces remained after impact. Microscopical examination of various fracture surfaces revealed surface crack initiation on 90% of the pieces. Brilliant color patterns, similar to a rainbow pattern, were present on all fracture faces. Descriptive photographs were not possible due to glaring fracture features. After a time lapse of one day, approximately 50% of the initial colors were present. Thus, 50% of the color patterns might be due to diffraction, i.e., interference phenomena, while the portion that decayed in one day, might be due to an "oriented layer" as often seen in PMMA.[22] Plastic deformation in glass is not predicted by Griffith's work but proposed more recently by Marsh[33] and Bridgman and Simon.[34] Further studies in glass fracture might help to prove or disprove plastic flow in glass. Continued studies in this area were discouraged by surface flaws, difficulty in flattening the rod ends, and in availability of lower bullet energies. Loads less than C.B. caps are mandatory for a detailed investigation in glass using this apparatus.

A machined inert rocket propellant rod was ballistically loaded with a 22 Winchester Magnum Rim Fire (Full Metal Case) without any optical damage. Testing in this area was discontinued due to the propellants high damping property. A design to accomodate a high power pistol or a rifle might produce fracture in propellants.

# VII. CONCLUSIONS

A simple economical device for producing high stress waves in materials was investigated, designed, and tested. With a shock wave definition as the guide line, i.e., an instantaneous pressure pulse, the ballistic impact-driven projectile was designed to introduce a semi-square compressive wave front, as shown in Figure 11. The steepness and sharpness of the wave front is solely dependent on the flatness of the impact surfaces, since short rods preclude sharpening of the wave due to its propagation through the rod, except for highly non-linear materials. Throughout the tests, the specimen and piston were kept as flat as possible. Spalling normal to the impact direction resulted when the reflected tensile component reached $\sigma_c$ for the particular flaw size in the rod. Three distinct fracture morphologies, i.e., inherent flaws, inclusions, and surface flaws, represented all fracture modes in PMMA rods. Associated with each fracture region were degrees of roughness, i.e., mirror, mist and hackle, or mirror and ribs. Each degree of roughness is related to some crack velocity, i.e., smooth surfaces correspond to low velocities while rough surfaces result from fast velocities. This seems possible since at the initiation of fracture, the crack moves slowly through the material. As the crack grows, its velocity increases until some critical velocity is reached, and brittle fracture results.

Cumulative fatigue loading in PMMA was not reproducible from

one sample to another. This variance in tests is due to PMMA irregularity and not to the test apparatus. No relation of fracture morphology as a function of number of loads was observed in the PMMA rods.

Other materials were examined to determine the range offered by this design. Urethane fractured producing an intricate crack geometry. Glass was shattered into many indistinguishable pieces. Inert rock propellants damped the wave magnitude before fracture could occur. In general, the design is suitable for studying spalling fractures due to high waves in a variety of materials.

REFERENCES


1. G. E. Duvall, Response of Metals to High Deformation, New York: Interscience Publishers, 1961.

2. W. P. Mason, "Internal Friction, Plastic, Strain, and Fatigue in Metals and Semiconductors," presented at Symposium on Basic Mechanisms of Fatigue, Boston, Massachusetts, June 23, 1958.

3. W. B. Benedick, "Nitroquanidine Explosive Plane-Wave Generator for Producing Low Aplitude Shock Waves," Rev. Sci. Instrum. 36, 1309 (1965).

4. C. H. Karnes, "The Plate Impact Configuration for Determining Mechanical Properties at High Strain Rates," presented at Symposium on the Mechanical Behavior of Materials under Dynamic Loads, San Antonio, Texas, September 1967.

5. A. A. Griffith, "The Phenomena of Rupture and Flow in Solids," Phil. Trans., Royal Soc., London, Series A, 221, 163 (1921).

6. F. A. McClintock and A. S. Argon, Ed., Mechanical Behavior of Materials, Reading, Massachusetts: Addison-Wesley Publishing Company, Inc., 1966.

7. C. E. Inglis, "Stresses in a Plate due to the Presence of Crack and Sharp Corners," Trans., Inst. Nav. Architects, 60, 219 (1913).

8. E. Orowan, "Energy Criteria of Fracture," Welding Res. Suppl. 20, 157 (1955).

9. G. R. Irwin, Fracturing of Metals, Cleveland, Ohio: American Society for Metals, 1948.

10. M. L. Williams, "Initiation and Growth of Viscoelastic Fracture," Int. J. of Fracture Mech., 1, No. 4, 1967.

11. W. B. Jones, "Cohesive and Adhesive Polymer Fracture Investigation," Ph.D. Dissertation, Department of Mechanical Engineering, University of Utah, June 1970.

12. P. L. Pratt, Ed., Fracture (1969), Proceedings of the Second International Conference on Fracture, 881, London: Chapman and Hall, Ltd. 1969.

13. G. J. Lake and P. B. Lindley, "Role of Ozone in Dynamic Cut Growth of Rubber," J. Appl. Polymer Sci., 9, 2 (1965).

14. E. H. Andrews, "Stresses at a Crack in an Elastomer", Proc. Phys. Soc., 77, 483 (1961).

15. H. Kolsky, Stress Waves in Solids, New York: Dover Publications, 1963.

16. B. D. Coleman, M. E. Gurtin and I. Herrera, R., "Waves in Materials with Memory, I. The Velocity of One-Dimensional Shock and Acceleration Waves," Arch. Rational Mech. Anal., 19, 1 (1964).

17. G. A. Secor, Private communications.

18. B. Rosen, Fracture Processes in Polymeric Solids, New York: John Wiley and Sons, Inc., 1964.

19. J. P. Berry, "Fracture Processes in Polymeric Materials. I. The Surface Energy of Poly (Methyl Methcrylate)", J. Polymer Sci., 50, 107 (1961).

20. J. P. Berry, "Fracture Processes in Polymeric Materials, III. Topography of Fracture Surfaces of Poly (Methyl Methacrylate)," J. Appl. Phys., 33, 5 (1962).

21. E. H. Andrews, Fracture in Polymers, New York: American Elsevier Publishing Company, Inc., 1968.

22. J. P. Berry, "Surface Characteristics of Fractured Poly (Methyl Methacrylate)," Nature, 185, 91 (1960).

22. F. Zandman, "Etude de la Deformation et de la Rupture des Matieres Plastiques," Publications Scientific et Technique due Ministere de l"Air, No. 291, Paris, 1954.

24. J. A. Kies, S. B. Newman, and I. Wolock, in Fracture, B. L. Averbach, D. K. Felback, G. T. Hahn, D. A. Thomas, Eds., New York: John Wiley and Sons, Inc., 1959.

25. H. Schardin, "Untersuchung von Zerreissvorgangen bei Kunststoffen," Kunststoffe, 44, 48 (1954).

26. L. J. Broutman and F. J. McGarry, "Fracture Surface Work Measurements on Glassy Polymers by a Cleavage Technique, II. Effects of Crosslinking and Preorientation," J. Appl. Polymer Sci., 9, 609 (1969).

27. J. P. Berry, "Fracture Processes in Polymeric Materials, IV. Dependence of the Fracture Surface Energy on Temperature and Molecular Structure," J. Polymer Sci., Part A, 1, 993 (1963).

28. E. E. Ziegler and W. E. Brown, Plastics Technical Service Bulletin, Midland, Michigan: Dow Chemical Company, 1954.

29. R. P. Kambour, "Optical Properties and Structure of Crazes in Transparent Glassy Polymers," Nature, 195, 1299 (1962).

30. R. P. Kambour, "Refractive Indices and Compositions of Crazes in Several Glassy Polymers," J. Polymer Sci., Part A, 2, 4159 (1964).

31. D. K. Roylance, "An EPR Investigation of Polymer Fracture," Ph.D. Dissertation, Department of Mechanical Engineering, University of Utah, August 1968.

32. D. J. Wulpi, How Components Fail, Metals Park, Ohio: American Society for Metals, 1966.

33. D. M. Marsh, Flow and Fracture in Glass in Fracture of Solids, D. C. Drucker, Ed., New York: Interscience Publishers, 1963.

34. P. W. Bridgman and I. Simon, "Effects of Very High Pressures on Glass," J. Appl. Phys. 24, 405 (1953).

# VITA

| | |
|---|---|
| Name | Dolores Labranche Simonson |
| Age | 25 |
| Education | B.S. Metallurgical Engineering with a Materials Science Option<br>Montana College of Mineral Science and Technology, 1966 |
| | M.S. Mechanical Engineering<br>University of Utah, 1970 |
| Honors | Anaconda Company Undergraduate Scholarship<br>1963-1966 |
| | N.S.F. Undergraduate Research Scholarship<br>1966 |
| | N.S.F. Graduate Fellowship<br>1969 |
| | Honorable Mention in A.S.M. Metallography Exhibit, 1967 |
| Experience | |
| Research | Undergraduate Research Assistant, N.S.F. Contract on Ternary Phase Diagram Study of Al-Ag-In. 1965-1966 |
| | Graduate Research, N.S.F. Contract on Cumulative Shock Fatigue, 1968-1969 |
| Industrial | Associate Engineer, Westinghouse Atomic Power Division, Pittsburgh, Pennsylvania<br>1966-1968 |
| Publications | Labranche, D. A., "Examination of Some Al-Ag-In Alloys," unpublished bachelor's thesis, Montana College of Mineral Science and Technology, 1966. |
| | Labranche, D. A. and Aqua, E. N., "Replicas for Porosity Determination in Sintered Uranium Dioxide," Westinghouse Atomic Power Division - 7058, June 1967 |